Memristive functionality based on viscous magnetization dynamics

Sergei Ivanov[1] and Sergei Urazhdin[1a)]
[1]*Department of Physics, Emory University, Atlanta, GA, USA.*

(Dated: September 26, 2022)

In viscous dynamics, velocity is proportional to the force. Ideal memristor is a device whose resistance changes at a rate proportional to the driving input. We present proof-of-principle demonstration of the connection between viscous dynamics and memristive functionality by utilizing a thin-film ferromagnet/antiferromagnet bilayer, where viscous magnetization dynamics results from the frustration at the magnetic interface, and driving is provided by external magnetic field. Thanks to the atomic scale of frustration effects, the presented approach is amenable to downscaling. It can be also adapted for electronic driving by spin torque, making it attractive for applications in neuromorphic circuits.

Introduction. Synapses in neural networks are connections that pass electrical and/or chemical signals between neurons and whose strength depends on the signal history, providing simultaneous computational and memory functionality. Memristors - two-terminal electronic devices whose resistance depends on their input history - are the most promising candidates for the hardware implementation of synapses in artificial neural networks[? ? ?]. According to the original definition[? ? ?], a memristor can be described by the equation

$$V(t) = R(Q)I(t) \tag{1}$$

where $R(Q)$ is the resistance, $I(t)$ is the input current, $V(t)$ is the output signal, and $Q = \int_0^t I(\tau)d\tau$. This definition has been extended to a much broader class of generalized memristors state described by V is driven by the generalized force (driving input) I. This generalization reflects the interchangeability of input and output types via, for example magneto- or optoelectronic effects. For instance, in the experimental demonstration discussed below, we for simplicity utilize magnetic field as the input driving the memristor via Zeeman coupling. This approach is equivalent to current driving, since current can be converted to the magnetic field via Ampère's law. At the nanoscale, direct current driving can be implemented using spin torque[?].

The dependence $R(Q)$ of resistance on charge is the essential feature of memristors providing the memory of the electrical history of the device. If this dependence is non-monotonic, this functionality becomes lost since a finite charge transfer may not change the resistance. Conversely, one can argue that the most efficient, "ideal" memristive performance is provided by the linear dependence of resistance on charge,

$$R(t) = R_0 + a\int_0^t I(\tau)d\tau. \tag{2}$$

where R_0 and a are constants.

For a periodic input signal (inset in Fig. 1), the solution of Eqs. (1)-(2) is a pinched V-I hysteresis loop (Fig. 1(a)). The R-I loop is lens-shaped for the triangular input waveform (Fig. 1(b)).

According to Eq. (2), the area of the R-I hysteresis loop (Fig. 1(b)) increases linearly with the period of the input signal, or equivalently decreases inversely with the sweep rate

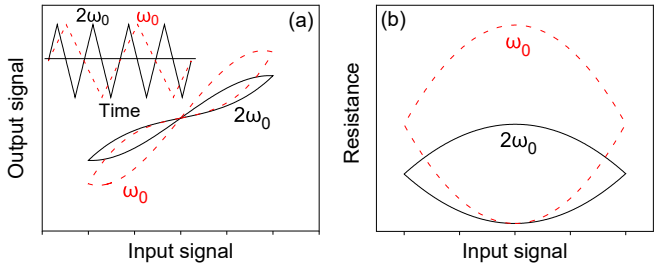

Figure 1. Characteristics of an memristor. (a) Output vs input signal, (b) Resistance vs input signal, for two different frequencies of the periodic triangular input (inset), as labeled.

ω, as shown in Fig. 1(b) for two values of ω. We note that Eq. 2 is unphysical, as it implies that $R < 0$ can be achieved for $aI < 0$. However, it may be possible to achieve an approximately integral dependence of R on the input over some range of the latter in a device exhibiting memristive behavior.

Here, we present a proof-of-principle experimental demonstration of memristive functionality approximately described by Eq. (2). Our approach is based on the observation that the memristive behavior in the differential form $\frac{dR}{dt} = aI(t)$ can be interpreted as a viscous response of R to the input I. Here, we use the term "viscous" by analogy to Newton's law in the presence of viscous friction, $m\ddot{x} + \nu\dot{x} = F_{ext}(t)$, where F_{ext} is the external force, and ν is viscosity. At small Reynolds numbers, it is reduced to $\dot{x} = F_{ext}(t)/\nu$, similar to Eq. (2) for the memristor.

We expect that memristive functionality can be achieved using a variety of physical implementations of viscous dynamics of mechanical, electronic, or magnetic degrees of freedom. Since the latter do not require physical motion, they generally exhibit superior endurance, repeatability, and reproducibility, which has motivated extensive exploration of magnetic generalized memristors. The most common design is based on the domain wall (DW) pinned at various positions in a magnetic nanowire incorporated into a magnetic tunnel junction[?]. However, DW motion becomes increasingly discrete at nanoscale, and either requires an input threshold or is randomized due to thermal fluctuations. These issues detrimental to memristive functionality can be described as deviations from viscous DW motion.

Another recent approach utilizes a dry friction-like effect of magnetization pinning in a nanoscale tunnel junction by

a)Electronic mail: surazhd@emory.edu

the high density of pinning centers in ferromagnets (Fs) sandwiched with thin-film antiferromagnets (AFs)[? ? ?]. This approach is amenable to downscaling, but unlike viscous friction, dry friction entails a significant input threshold for the dynamical response, compromising memristive behaviors and device efficiency.

F/AF systems have been extensively studied in the context of exchange bias (EB) - unidirectional asymmetry of the magnetic hysteresis loop[?]. It is well established that thick AF in F/AF bilayers form a multidomain state to accommodate frustrated exchange interaction at the F/AF interface[?]. Frustration in sufficiently thin AFs was predicted to result in the formation of a "Heisenberg domain state" (HDS) that consists of tightly-packed AF DWs[? ? ?], but until now the implications for the dynamical magnetic properties have remained virtually unexplored.

In AF alloys such as IrMn utilized in Ref.[?], the magnetization dynamics is likely dominated by pinning on magnetic defects associated with variations of local stoichiometry, resulting in dry friction-like behaviors. In contrast, time-domain and ac susceptibility measurements in Fs sandwiched with high-quality AFs CoO and NiO demonstrated viscous AF dynamics close to EB blocking temperature T_B[? ? ? ?]. At lower temperatures, viscosity was shown to rapidly increase, leading to magnetic freezing. Thus, HDS was identified as a correlated spin glass, i.e. the state that exhibits local magnetic ordering but lacks long-range magnetic order. Such a state can be particularly advantageous for memristive applications, since exchange interaction that underlies the frustration is large, provides a large-scale energy landscape that can stabilize a multitude of spin states even in nanoscale devices. Importantly, the spin liquid state at temperatures above the glass transition is expected to be characterized by a hierarchical multi-scale energy landscape, enabling viscous magnetization dynamics dynamics that can be efficiently driven by small inputs. Here, we build on these findings to demonstrate proof-of-principle memristive functionality in the viscous state of a thin-film bilayer of Permalloy (Py) with NiO.

Model. To facilitate the analysis of memristive behaviors in F/AF heterostructures, we introduce a model for the viscous dynamics of AF coupled to F. In our experiment, the resistive signal is provided by the anisotropic magnetoresistance (AMR) - the 180°-periodic dependence of R on the angle between the electric current $\vec{I}$ and the magnetization $\vec{M}_F$ of F. The relevant angles, measured relative to the fixed x-axis, are introduced in the inset in Fig. 2(b): φ is the angle of the magnetic field $\vec{H}$, $\theta_F(\theta_{AF})$ is the angle of $\vec{M}_F(\vec{M}_{AF})$. Here, $\vec{M}_{AF}$ is the uncompensated magnetization of AF at the interface with F, producing effective exchange field $\vec{H}_{AF} \parallel \vec{M}_{AF}$. The current $\vec{I}$ is directed at a fixed angle of 45°.

The AMR can be linearized around $\theta_F = 0$,

$$R(\theta_F) = R_0 + \Delta R \sin^2(\theta_F + \frac{\pi}{4}) \approx R_0 + \frac{\Delta R}{2} + \Delta R \theta_F, \quad (3)$$

where R_0 is the AMR minimum, and ΔR is the magnetoresistance.

On timescales significantly larger than that of intrinsic dynamics of F, the direction of $\vec{M}_F$ is determined by the balance between the torques exerted by $\vec{H}$ and $\vec{H}_{AF}$[?],

$$\vec{H} \times \vec{M}_F = \vec{M}_F \times \vec{H}_{AF}. \quad (4)$$

This equation can be rewritten in terms of the relevant angles as

$$H(t)\sin(\varphi(t) - \theta_F(t)) = H_{AF}\sin(\theta_F(t) - \theta_{AF}(t)). \quad (5)$$

When the external field is zero, the magnetization of ferromagnet aligns with the interfacial uncompensated magnetization of antiferromagnet, resulting in $\theta_F = \theta_{AF}$ in equilibrium. For AF, we assume viscous dynamics of uncompensated magnetization described by the magnetic viscosity constant ν and driven by the exchange interaction with F,

$$\nu \frac{d\theta_{AF}(t)}{dt} = \sin(\theta_F(t) - \theta_{AF}(t)). \quad (6)$$

where $\nu \propto \frac{\alpha}{\gamma}$, α is the Gilbert damping, and γ is the gyromagnetic ratio, is obtained from Landau–Lifshitz–Gilbert–Slonczewski equation (LLGS) in the overdamped limit $\alpha \gg 1$[?]. The dynamics of the system involves coupled evolution of F and AF described by Eqs. (5) and (6). For concreteness, assume that the system is initially prepared in the state $\theta_F = \theta_{AF} = 0$, and a time-dependent magnetic field $H(t)$ is applied at angle $\varphi = 90°$ starting at $t = 0$. To the lowest order in θ_{AF}, the solution of Eq. (6) is

$$\theta_{AF}(t) \approx \frac{1}{\nu H_{AF}} \int_0^t H(t')dt'. \quad (7)$$

For the sinusoidally varying driving magnetic field $H(t) = H_0 \sin\frac{2\pi t}{\tau}$,

$$\theta_{AF}(t) = \frac{\tau H_0}{\pi \nu H_{AF}}(1 - \cos\frac{2\pi t}{\tau}) \quad (8)$$

resulting in an elliptic R-H hysteresis loop with an area

$$S = \Delta R \frac{\tau H_0^2}{\nu H_{AF}}, \quad (9)$$

proportional to the period τ of the input and inversely proportional to the magnetic viscosity. A similar result is obtained for the triangular driving signal, establishing the connection with the memristor, see Fig. 1(b).

Methods. The studied sample with the structure NiO(8 nm)/Py(10 nm)/Ta(5 nm) was deposited on an oxidized Si substrate by high-vacuum magnetron sputtering at room temperature. NiO was deposited by reactive sputtering from a Ni target in Ar/O_2 mixture, with the partial oxygen pressure adjusted to optimize the magnetic properties, as in our previous studies of NiO and the structurally similar CoO[? ? ? ?]. Py and Ta were deposited in ultrahigh purity Ar. The Ta capping layer was used to protect the structure from oxidation. The deposition was performed in $\approx$ 100 Oe in-plane field known to facilitate well-defined exchange anisotropy in F/AF bilayers.

The thickness of NiO was adjusted to achieve the EB blocking temperature $T_B \approx 90$ K well within the experimentally accessible range, allowing us to analyze the viscous

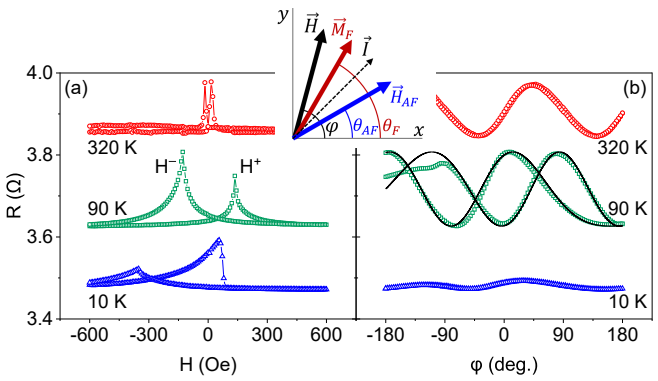

Figure 2. Magnetoelectronic hysteresis loops obtained by varying a field with a fixed $\varphi = -45^\circ$ (a), and by rotating a fixed field $H = 180$ Oe at a rate of $3\frac{\text{deg.}}{\text{s}}$ (b), at the labeled values of T. The data in (b) are offset for clarity. Curves in (b) are calculations as described in the text, with $\nu = 13$ s, $H_{AF} = 155$ Oe. Inset: schematic of the relevant angles.

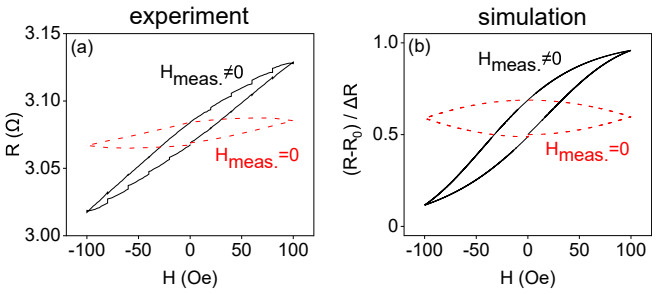

Figure 3. (a) R vs H (solid curve) and $R(H = 0)$ (dashed curve) measured at $T = 90$ K. (b) Simulated R vs H (solid curve) and $R(H = 0)$ (dashed curve). The plotted quantities are defined in the text.

magnetization dynamics expected at temperature around T_B. Thicker NiO is expected to enable room-temperature device operation[?], making the device more suitable for practical applications. A detailed study of the parameter optimization possibilities is left for future research. The roughness of magnetic layers, characterized by atomic force microscopy on separate samples, where deposition was terminated at the respective layer, was ≤ 0.35 nm rms.

Magnetoelectronic measurements were performed in the 4-probe van der Pauw geometry, using ac electric current $I = 0.1$ mA rms at frequency $f = 1.3$ kHz, and lock-in detection. To initialize the system in a well-defined magnetic state, it was cooled in a constant magnetic field $H = 400$ Oe oriented at $\varphi = 0$ (see inset in Fig. 2). The magnetic properties of the system were characterized by magnetoelectronic measurements of the hysteresis loop obtained by sweeping the field at $\varphi = -45^\circ$ corresponding to the minimum of AMR (Fig. 2(a)), and by the response to rotating field of fixed magnitude (Fig. 2(b)).

Characterization. The peaks in the hysteresis loops (Fig. 2(a)) at fields H^+ and H^-, are associated with the reversal of M_F, allowing us to determine the coercivity $H_C = \frac{H^+ - H^-}{2}$ and the effective EB field $H_E = -\frac{H^+ + H^-}{2}$ (Fig. 2(a)). At the temperature $T = 320$ K$\gg T_B = 90$ K, $H_E = 0$ and the coercivity is small. The coercivity is enhanced at $T = 90$ K $= T_B$, but H^+ and H^- remain symmetric. The asymmetry of reversal points at $T = 10$ K $< T_B$ is associated with the onset of EB, resulting in a finite $H_E \approx 160$ Oe. These behaviors are consistent with prior studies of F/AF bilayers based on NiO and other AF materials[? ? ?].

Figure 2(b) shows the response to a rotating field $H = 180$ Oe. At $T = 320$ K, the dependence $R(\varphi)$ is sinusoidal and the hysteresis with respect to the direction of rotation is negligible, as expected for M_F aligned with the rotating field. At $T = 90$ K $= T_B$, the dependence remains sinusoidal, consistent with the absence of directional anisotropy, but a large hysteresis appears with respect to the rotation direction. Similar hysteretic behaviors have been reported at T_B for other F/AF systems and interpreted in terms of rotating exchange anisotropy[? ?]. At $T = 10$ K, the resistance remains almost constant, indicating that M_F is pinned by EB.

The hysteretic response to the rotating field at $T = 90$ K shown in Fig. 2(b) indicates that the state of the magnetic system is history-dependent, as required for the memristive functionality. In particular, these data show that the value of R at $\varphi = 0$ can vary over almost the entire range of AMR, i.e. the metastable orientations of $\vec{M}_F$ span the range of almost 180° even at a relatively large $H = 180$ Oe oriented at $\varphi = 0$. These data are well described by the model of viscous AF magnetization dynamics introduced above, as shown by the curves in Fig. 2(b) obtained by solving Eqs. (5), (6).

Memristive functionality. We now experimentally demonstrate that the studied structure exhibits memristive functionality at temperatures above $T_B = 90$ K, and confirm its origin from viscous AF magnetization dynamics.

To test the memristive functionality, the system is initialized in a state with $\theta_F = \theta_{AF} = 0$, corresponding to the middle of the linear part of AMR, by in-field cooling. Magnetic field perpendicular to the magnetization ($\varphi = 90^\circ$) is subsequently periodically swept in a triangular wave pattern, and the sample resistance is simultaneously measured.

A solid curve in Fig. 3(a) shows the R vs H hysteresis loop obtained at $T = 90$ K by sweeping H between -100 Oe and 100 Oe with a period of 100 s. Its shape is reminiscent of the lens-shaped hysteresis curve expected for a memristor (Fig. 1(b)), but is tilted. The tilt can be explained by the hybrid nature of the magnetic system, where the AF providing memristive functionality is coupled only indirectly to the driving field via F.

To directly access the state of AF, we modified the measurement protocol to remove the external field prior to each measurement during the sweep. Since the intrinsic dynamics of F occurs on significantly shorter timescales than our measurement, M_F aligns with M_{AF}, so the state of AF is revealed by such measurements. This modified approach almost completely eliminated the tilt of the hysteresis loop (dashed curve $R(H = 0)$ in Fig. 3(a)), confirming its origin from the hybrid nature of the magnetic system. Simulations based on the model of viscous dynamics introduced above reproduces the salient features of these results (Fig. 3(b)).

The hysteresis in Fig. 3 demonstrates generalized memristive functionality - dependence of resistance on the history of the applied magnetic field used as the driving input in our proof-of-principle experiment. To investigate whether the response is consistent with the behaviors expected for memristors, we analyze the dependence of the area under the hysteresis loop on the period of the field sweep. An "ideal" memristor with a linear $R(Q)$ is expected to exhibit a linear dependence of R on the period of the driving input, as discussed above.

Figure 4(a) shows the measured dependences of the area of the R vs H hysteresis loop on the period of the input, for $T = 90-120$ K. These data show that the measured area increases with the period of the input, as expected for the memristor with linear $R(Q)$, but the dependence is nonlinear. The area also increases with increasing T, consistent with the expected decrease of magnetic viscosity with increasing temperature.

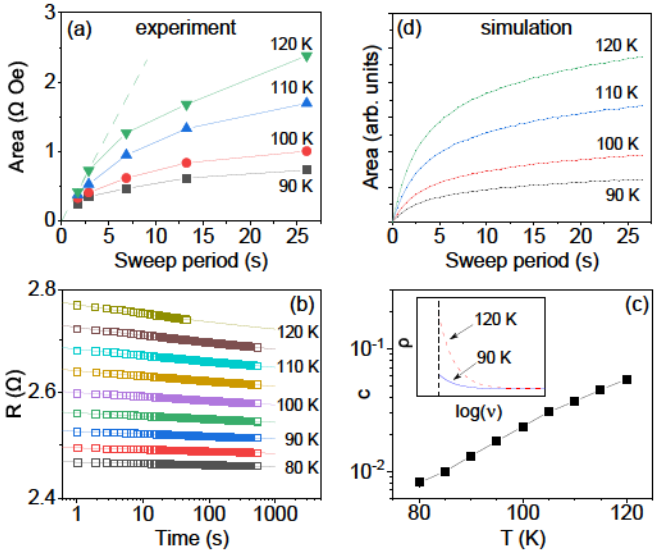

Figure 4. (a) Measured dependence of the area of the R vs H hysteresis loop on the period of the applied field sweep, at the labeled values of T. (b) Symbols: R vs time recorded after abruptly rotating the field $H_0 = 100$ Oe from $\varphi = 45°$ to $\varphi = -45°$, at the labeled values of T. Curves: fitting with $R(t) = R(\infty) + At^{-c}$. (c) Dependence of the power-law exponent c on T. Inset: distribution of viscosity extracted from the aging data, for two values of T. (d) Dependence of the area under the $R-H$ hysteresis loop on the period of the input signal, simulated using the magnetic viscosity distribution determined from the aging data.

We now show that the deviations from the linear behaviors manifested by the nonlinear dependences in Fig. 4(a) can be explained by the inhomogeneity of viscous AF dynamics, resulting in a distribution of viscosity ν. Such inhomogeneity may result from the local variations of the AF thickness and/or from the inherent local variations of the effects of frustration due to random exchange at F/AF interface.

To determine the distribution $\rho(\nu)$ of the magnetic viscosity, we performed separate measurements of magnetic aging, in which the magnetic field was abruptly rotated, and subsequently the time-dependent resistance of the sample was monitored at a fixed field $H_0 = 100$ Oe. Aging in these systems has the same mechanism as the proposed memristive behaviors. Namely, it is associated with viscous evolution of AF magnetization under the influence of the exchange torque from the magnetization of F, when the latter is twisted by external field or spin torque. For a system characterized by a single value of viscosity ν, the resistance dependence predicted by our model is

$$R(t) - R(\infty) \approx \Delta R \left(\frac{H_{AF}^2}{H_{AF}^2 + H_0^2} \right) e^{-\frac{2H_0}{\nu(H_0+H_{AF})}t}, \qquad (10)$$

where $R(\infty)$ is the asymptotic value of R corresponding to $\vec{M}_F \parallel \vec{H}_0$.

As shown in Fig. 4(b), aging does not follow the exponential dependence of Eq. (10), but can be well-fitted by the power-law dependence on time, in the form $R(t) = R(\infty) + At^{-c}$, where A and c are constants. Power-law dependence indicates that there is no characteristic time scale in the system, i.e. no single viscosity value, but a distribution of viscosity throughout the sample. An alternative, or a co-existing, possible mechanism is a broad distribution of the effective exchange field H_{AF}, which enters Eq. (10) on equal footing with ν.

We note that the observation of aging provides definitive proof for viscous dynamics, as opposed to dry friction[? ?]. Indeed, once the dry friction is overcome at sufficiently large H_0, the magnetic system would rapidly evolve and relax over the intrinsic dynamical scales of order nanosecond. The measured power-law aging can be interpreted as a superposition of contributions from the exponential aging associated with a particular value of ν, and characterized by the distribution $\rho(\nu)$[?],

$$R(t) - R(\infty) = At^{-c} \propto \int_0^\infty \rho(\nu) e^{-\frac{2H_0}{\nu(H_0+H_{AF})}t} d\nu. \qquad (11)$$

The distribution is normalized by

$$\int_{\nu_{min}}^\infty \rho(\nu) d\nu = 1, \qquad (12)$$

where ν_{min} is the cutoff. Formally, a cutoff is needed to ensure convergence. Physically, at short timescales corresponding to small ν, the system must crossover from viscous to damped dynamics. The dependence Eq. (10) becomes inapplicable in this regime. We use the value $\nu_{min} = 0.1$ s which is below the shortest timescales in our measurements, and does not influence the quality of fitting.

Inverse Laplace transform yields Pareto distribution for the viscosity,

$$\rho(\nu) = \frac{c\nu^{-(c+1)}}{\nu_{min}^{-c}}. \qquad (13)$$

The distribution extracted from the data is shown in the inset of Fig. 4c for two values of T. The power-law exponent c rapidly increases with temperature (Fig. 4(c)). According to Eq. (13), this implies a redistribution of $\rho(\nu)$ towards smaller values of ν, consistent with the expected decrease of viscosity.

Figure 4(d) shows the simulated dependences of the R-H hysteresis loop area on the period of the field sweep and temperature, obtained using the distribution of viscosity determined from the aging data. These results reproduce the observed deviations from the linear memristive behaviors (Fig. 4(a)), supporting the proposed interpretation in terms of the inhomogeneous distribution of viscosity.

I. SUMMARY

We have experimentally demonstrated generalized memristive behaviors in a thin-film F/AF bilayer, where frustration at the F/AF interface leads to viscous dynamics of magnetization. We showed that viscous dynamics results in the integral dependence of device resistance on its input, consistent with the original definition of a memristor. The demonstrated devices exhibit deviations from the linear behaviors, which can be explained by the distribution of viscosity associated with the frustrated nature of the studied system.

In our proof-of-principle demonstration, external magnetic field was utilized as the input driving the magnetization dynamics, and anisotropic magnetoresistance was utilized as the mechanism to convert this dynamics into resistance variations. For applications, the structures must be downscaled to nanometer dimensions. The demonstrated viscous behaviors are expected to persist down to nanoscale, because frustration underlying such viscous behaviors is associated with the atomic-scale incompatibility between ferromagnetic and antiferromagnetic ordering, which is expected to result in a complex magnetic energy landscape even at nanoscale. Anisotropic magnetoresistance utilized in our measurements is too small for practical applications. Magnetoresistance in magnetic tunneling junctions based on similar thin-film F/AF bilayers can provide much larger signals. Such devices can be efficiently driven by spin torque instead of the external magnetic field, resulting in memristive response to current amenable to integration into electronic circuits. Current-controlled devices can implement a second-order memristors[?], in which Joule heating transitions the system between the frozen idle state and the viscous active state discussed in this paper.

An important issue related to the practicality of the proposed memristors is whether the magnetic frustration underlying viscous dynamics will result in large device-to-device variations at the nanoscale. While such crossover must inevitably occur on atomic lengthscales, a prior observation that aging in similar F/AF heterostructures is associated with collective dynamics[??] is encouraging, since it implies that the effects of individual magnetic defects and pinning centers are averaged by internal magnetic interactions. Along with the well-known high endurance of magnetic devices, the demonstrated memristive behaviors can make the proposed devices based on viscous magnetization dynamics well-suited for the hardware implementation of artificial neural networks.

II. ACKNOWLEDGMENTS

This work was supported by NSF awards ECCS-1804198 and ECCS-2005786.

The data that support the findings of this study are available from the corresponding author upon reasonable request.

REFERENCES